Nanoscale

COMMUNICATION

View Article Online
View Journal | View Issue

Cite this: *Nanoscale*, 2015, **7**, 18049

Received 14th August 2015,
Accepted 5th October 2015

DOI: 10.1039/c5nr05514h

www.rsc.org/nanoscale

Packaged triboelectric nanogenerator with high endurability for severe environments†

Long Gu,[a] Nuanyang Cui,[a] Jinmei Liu,[a] Youbin Zheng,[a] Suo Bai[a,b] and Yong Qin*[a,b]

Many factors in the environment (such as dust, moisture and rain) severely influence the output performance of a triboelectric nanogenerator (TNG), which greatly limits its application. In this work, we designed and fabricated a kind of packaged TNG (PTNG) that can work normally in dust and humidity for harvesting noise energy. Under a sound wave of 110 dB and 200 Hz, the PTNG can generate a maximum output voltage of 72 V and a maximum output current of 0.66 mA. In the structure of the PTNG, the frictional layers are fully isolated from the ambient environment, which makes it work steadily in dusty and humid conditions without any damping of the output performance. Moreover, it can be used as a stable power source to directly light up 24 red commercial light emitting diodes (LEDs) driven by sound even in a severely rainy environment. This PTNG has great potential to be applied in real environments, which is critically important to the application of TNGs.

Introduction

In the past few decades, more and more efforts have been devoted to harvesting mechanical energy from the ambient environment to get a sustainable power supply for tremendous micro/nanodevices.[1–8] As a common form of mechanical energy, sound energy exists anywhere and at any time in our environment, but is often wasted owing to a lack of effective harvesting methods.[9,10] Although sound energy has been scavenged by approaches based on the piezoelectric effect[11–13] and electrostatic effect[14] in previous works, their application is limited by their low energy conversion efficiencies,[11,12] complex structures[13] and high requirements for materials.[14] Recently, the newly invented triboelectric nanogenerator has been proved to be a simple, low-cost and effective technology to harvest various forms of mechanical energy and convert them into electric energy.[15–24] The energy conversion is achieved by coupling between triboelectrification and electrostatic induction. When two materials with different triboelectric polarities contact and rub against each other, surface charge will transfer from one material to the other. Then the periodic contact and separation of the oppositely charged surfaces can generate an induced potential difference between two electrodes, which drives an alternating flow of electrons through an external circuit. Lately, several works have been reported to harvest sound energy based on this technology.[25–27] Compared with the previously reported sound harvesters, the sound driven triboelectric nanogenerator (STNG) greatly improved the sound energy conversion efficiency and the output performance. But these STNGs have an open structure, which is commonly used in most reported TNGs. As the whole internal structure is exposed to the environment, these TNGs can't work normally in severe environments such as in dusty or moist environments. Dust can easily adsorb to the frictional surfaces of the TNG and hinder the contact of the frictional surfaces, resulting in a decrease in the TNG's output. In addition, the moisture adsorbed on the frictional surfaces can also increase the conductivity of the friction layers, and then discharging occurs on the surfaces, leading to a decrease in the TNG's output.[28] Thus, these factors in the environment could greatly influence the state of the frictional surfaces and reduce the output performance of the TNG. But a sound harvester needs to work under different environments, such as in a very humid place or a dusty region, or a rainy district. These diverse application conditions require the STNG to have a high endurability and the ability to work normally in these severe working conditions. Therefore, a sound harvester which has not only excellent output performance but also outstanding environmental stability in severe working conditions is urgently needed.

In this work, we developed a highly robust sound driven PTNG by integrating polyethylene (PE) film and a multihole polyvinyl chloride (PVC) plate. Its maximum output voltage

[a]*Institute of Nanoscience and Nanotechnology, School of Physical Science and Technology, Lanzhou University, Lanzhou, 730000, China.*
E-mail: qinyong@lzu.edu.cn
[b]*The Research Institute of Biomedical Nanotechnology, Lanzhou University, Lanzhou 730000, China*

†Electronic supplementary information (ESI) available. See DOI: 10.1039/c5nr05514h

and current can reach 72 V and 0.66 mA, respectively. By isolating the frictional surfaces of the PTNG from the ambient environment, it could work steadily in dusty and humid conditions. Moreover, it can stably and directly light up 24 red commercial LEDs without an energy storage process even in severely rainy condition.

Results and discussion

As schematically illustrated in Fig. 1a, the PTNG consists of four parts: a multihole PVC plate covered with a layer of Al (Al@PVC), a PE film with Ag electrode on one side and polyvinylidene fluoride (PVDF) nanofibers (the scanning electron microscope image is shown in Fig. 1b) on the other side (Part A), a PE film with Ag electrode on one side (Part B), and two spacers. These components are connected using double-side tape along their four edges to construct the drum-like PTNG. In the sealed structure, the multihole PVC plate acts as the skeleton of the PTNG, and the Al coated on it plays the dual roles of being a frictional surface and an electrode. A large number of through-holes in the PVC plate could greatly reduce the attenuation of sound when it propagates through the plate.

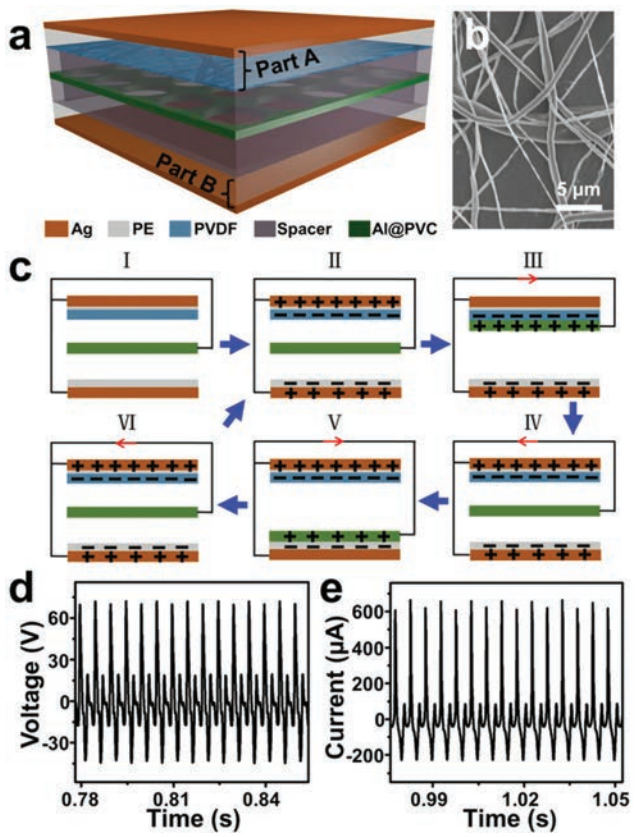

Fig. 1 (a) Structural illustration of the PTNG. (b) Scanning electron microscope image of the PVDF nanofibers. (c) Sketches of the electricity generation process in a full cycle. The red arrows indicate the direction of current. (d, e) The open-circuit voltage and short-circuit current of the PTNG.

The internal surfaces of Part A and Part B act as the frictional layers in the PTNG and hierarchically convert the sound energy, which improves the utilization efficiency. Moreover, Part A and Part B can fully isolate the frictional layers of the PTNG from the ambient environment realizing the effective protection of the device from negative influences. Two spacers connect Part A and Part B with the PVC plate, creating a cavity at the center between them for the vibration of Part A and Part B. Fig. 1c shows a full cycle of the electricity generation process of the PTNG. In the figure, the Al@PVC is replaced by a layer of Al to simplify the diagram. In the initial state, Part A and Part B are not in contact with the Al layer, and there is no charge existing on them (Fig. 1cI). When the device is driven by a sound wave, Part A and Part B will vibrate at the same frequency as the sound wave. Once the internal surface of Part A or Part B contacts and rubs against the Al layer, charge will transfer between them. According to the triboelectric series, electrons are injected from the Al to the PVDF in Part A and to the PE in Part B, generating negative triboelectric charges on the PVDF and PE (Fig. 1cII). When the PVDF in Part A is fully contacted with the Al layer (Fig. 1cIII), the Ag electrode in Part A possesses a higher electric potential than the Al electrode. As a result, the free charge flows from the Al electrode to the Ag electrode through the external circuit to balance the potential difference. Subsequently, the Al layer will reach the middle of Part A and Part B. Meanwhile, the electric potential of the Ag electrode in Part A drops and is lower than that of the Al electrode, so the charge flows back in the opposite direction, from the Ag electrode to the Al electrode (Fig. 1cIV). As the vibration continues, the Al layer then contacts with Part B (Fig. 1cV). In this state, the triboelectric charge on the PE induces a higher electric potential on the Ag electrode in Part B than on the Al electrode, which drives the free charge to flow from the Al electrode to the Ag electrode to screen the potential difference. When the vibration reverts back to state II, the distribution of charge returns to state II as well (Fig. 1cVI), and a cycle of the electricity generation process is fully completed. In summary, when Part A and Part B vibrate up and down, the PTNG acts as an electron pump that drives electrons to flow back and forth between the Ag and Al electrodes, producing an alternating current with four pulses in each period. Fig. 1d and e show the output voltage and current of the PTNG. Driven by a sound wave of 110 dB and 200 Hz, the PTNG generates an output voltage of 72 V and an output current of 0.66 mA. The period of the output signals is 5 ms, and two positive and two negative peaks can be observed in each cycle, which corresponds well with the PTNG working process discussed above.

In order to investigate the influence of environmental factors on the STNG, dusty, humid and rainy conditions were used as the working environments to test the output performance of the STNG. As a comparison, an unsealed TNG (UTNG) was also fabricated as a control group, which just contains one PE film with PVDF nanofibers, a multihole PVC substrate and a spacer. Compared with the PTNG, the PE film without the PVDF nanofibers is removed in the structure. Thus, the internal structure of the UTNG is completely exposed to the

environment. First of all, the impact of dust on the output performance of the UTNG and PTNG was investigated to examine the anti-dust capability of the PTNG. In this experiment, the two kinds of STNGs were both put into an enclosed box (25 cm × 25 cm × 18 cm) and then 0.2 g dust was blown into the space to guarantee that dust was deposited on the two STNGs with the same density. By repeating the above operation, we could deposit different amounts of dust on the two devices. For the UTNG, the dust particles could easily diffuse into its internal structure along with air, and then adsorb on its frictional surfaces. Fig. 2a shows the optical images of the PVDF nanofibers covered by 0, 3.2, 6.4, 9.6, 12.8, 16.0 g m^{-2} dust. It can be easily seen that more and more PVDF nanofibers are covered by dust particles with the increase of the dust density. These dust particles will severely hinder the contact of the PVDF with the Al, leading to a sharp decrease in the UTNG's output current (Fig. 2b). In this process, a sound wave of 103 dB and 200 Hz was used to drive the two STNGs. The statistical result in Fig. 2c shows that the current peak value of the UTNG decreases from 390 μA to 24.5 μA (it drops by 93.7%) after 16 g m^{-2} dust was deposited on the device. Meanwhile for the PTNG, the whole device is sealed and the dust cannot reach the internal frictional materials. Thus, its output current changes little with the increase of the dust density (Fig. 2d). The statistical result in Fig. 2e reveals that the current peak value of the PTNG keeps stable at about 560 μA all the time, which indicates that the PTNG is very dustproof and could work steadily in dusty environment.

Besides dust, moisture can influence the output performance of TNGs through changing the conductivity of the frictional layers. In order to examine the anti-humidity capability of the PTNG, the influence of humidity on the output performance of the UTNG and PTNG was investigated. In this part, the two devices were placed into an enclosed box with a controlled relative humidity (RH), and were driven by a sound wave of 90 dB and 200 Hz. Fig. 3a and b show the output current of the UTNG and PTNG with the RH ranging from 15% to 90% in steps of 15% at room temperature. The output current of the UTNG decreases with the increase of the RH, while the output current of the PTNG displays no change. As the RH increases from 15% to 90%, the current peak value of the UTNG decreases from 130 μA to 101 μA (it drops by 22.3%), while the current peak value of the PTNG remains at about 156 μA without any obvious change as shown in Fig. 3c. Furthermore, the RH in the box was increased to 100%, and then these two STNGs were kept in this condition for 5 hours. The corresponding output current of the UTNG decreases to about 45 μA (it drops by 65.4% compared with that at a RH of 15%), as shown in Fig. 3d, while the output current of the PTNG still remains at about 156 μA (Fig. 3d). These results indicate that the PTNG has an excellent performance when resisting moisture and could work steadily in a humid environment.

Except for dust and moisture, the STNG will still inevitably face some extreme conditions when it works outdoors, such as

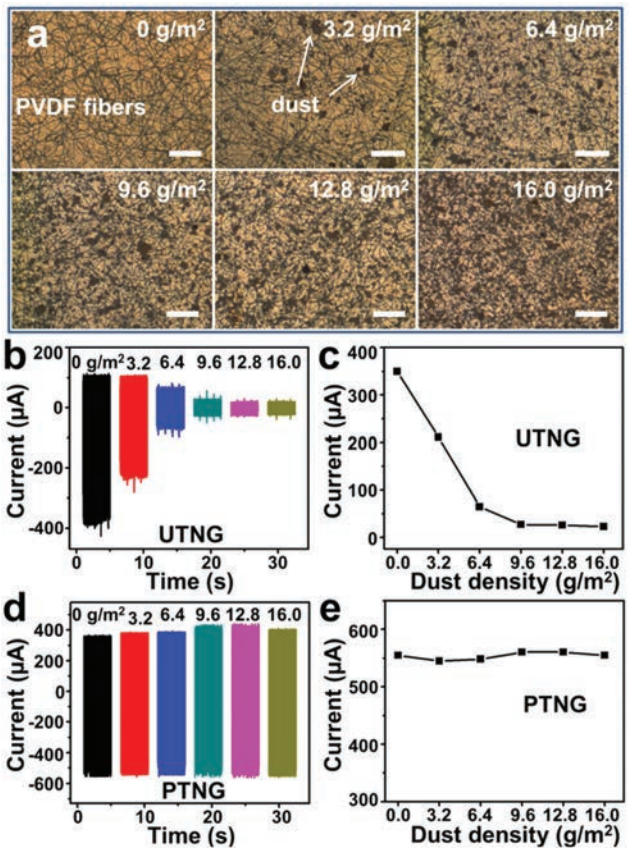

Fig. 2 (a) Optical images of the PVDF nanofibers on PE film covered by 0, 3.2, 6.4, 9.6, 12.8, 16.0 g m^{-2} dust, respectively. All scale bars are 100 μm. (b, d) The output current of the UTNG and PTNG under different dust densities. (c, e) The relationship between current peak values and dust density.

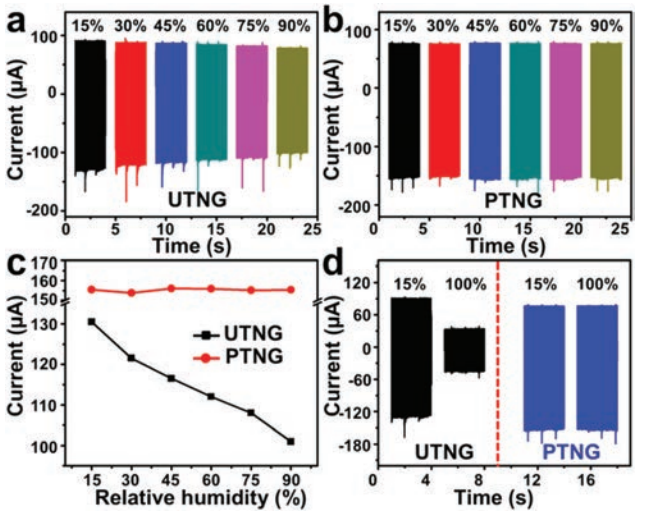

Fig. 3 (a, b) The output current of the UTNG and PTNG under different RHs. (c) The relationship between current peak values and RH. (d) The output current of the UTNG and PTNG at a RH of 15% comparing with their output current after being kept at a RH of 100% for 5 h. Percentages inset in (a), (b) and (d) are the RH at room temperature.

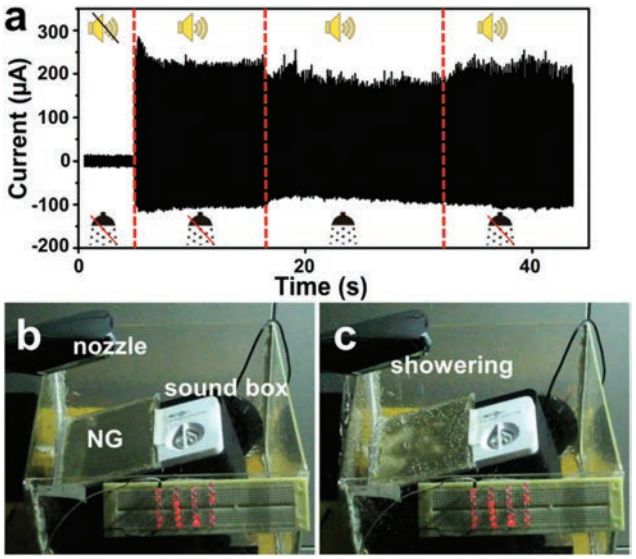

Fig. 4 (a) The output current of the PTNG under rainy condition simulated by a shower nozzle. (b, c) 24 red commercial LEDs lit up by the PTNG with the shower nozzle off (b) and on (c).

rain. A large amount of rainwater can promote the environmental RH to 100% and infiltrate into the internal structure of the TNG, which will greatly reduce the output performance of the TNG.[29] Here, rainy conditions were simulated by using a shower nozzle, and the output performance of the PTNG was measured in this case. As shown in Fig. 4a and Video S1,† the output current of the PTNG is about 230 μA before opening the shower nozzle. Once the nozzle is open, the water drops fall on the surface of the PTNG. Meanwhile, the output current of the PTNG decreases to about 180 μA. When closing the nozzle, the output current gradually returns to about 230 μA. The decrease and recovery of the output current in this process are attributed to the following reason. When the shower nozzle is on, the water drops fall on the surface of the PTNG and the weight on the PE films increases. Thus, the amplitude of the PE films decreases simultaneously, resulting in a small decrease in the PTNG's output. When the shower nozzle is closed, the water on the device will be flicked off by the vibrating PE films. Then the device returns to its original state and the output current reverts back as well. Although the output current of the PTNG is slightly decreased under the shower, it is still big enough to power many electronic devices. Here, the PTNG was used to power 24 red commercial LEDs (Fig. 4b). Obviously, the brightness of these LEDs changes little before and after the water drops fall on the PTNG as shown in Fig. 4c and Video S2,† which demonstrates that the PTNG could work normally in rainy circumstance as a stable power supply.

Conclusions

In summary, we developed a PTNG and investigated the influence of dust and moisture on its output performance. The maximum output voltage and current of the PTNG are up to 72 V and 0.66 mA, respectively. It works steadily in dusty and humid environments. Moreover, it can be used to stably light up 24 red commercial LEDs even in simulated rain. This kind of PTNG has great potential to be applied in severe environments such as in dusty, humid and rainy conditions, which paves the way for the practical application of triboelectric nanogenerators.

Experimental section

Fabrication of the PTNG

Firstly, a thin layer of Al is deposited on both sides of the multihole PVC plate (10 cm × 10 cm × 0.5 mm) by magnetron sputtering to get the Al coated PVC plate. Secondly, a piece of PE film (thickness of 5 μm) is covered by PVDF nanofibers on one side by electrospinning and deposited with Ag on the other side by magnetron sputtering, which is marked as Part A. Another piece of PE film is only deposited with Ag on one side by magnetron sputtering, which is marked as Part B. Thirdly, two spacers (thickness of 30 μm) are glued along the edges of the PVC plate on both sides. After that, Part A is glued on one spacer and Part B is glued on the other spacer with the Ag electrodes outside, as shown in Fig. 1a. Here, Part A and Part B have two roles. On one hand, both of their inner surfaces are used as the frictional surfaces to work with the Al on the PVC plate. On the other hand, they are used as the packing materials to pack the top and the bottom of the device, respectively. Finally, the fabricated device is sealed along the edges with sealant, which cooperates with the packing top of Part A and the packing bottom of Part B to realize a fully packaged structure. At the same time, the Ag deposited on Part A and Part B is connected together as one electrode and the Al deposited on the PVC plate acts as the other electrode for the subsequent electric measurements.

Electrospinning of the PVDF nanofiber

3.75 g PVDF, 8.5 g *N*,*N*-dimethylacetamide (DMAC) and 12.75 g acetone are mixed in a triangular flask and stirred at 60 °C for 30 min to form a uniform solution. Then the solution is added into a syringe. The electrospinning is conducted at 15 kV with a feed rate of 3 mL h^{-1}, and the distance between the needle and collector is 16 cm.

Controlling of RH

A humidifier, a mini fan and a thermohygrometer are installed into an enclosed box before measurement. The humidifier is used to adjust the moisture content, and the fan is used to speed up the uniform distribution of moisture in the space. The thermohygrometer is used to monitor the RH and temperature in the space. Through real-time monitoring and meticulous adjusting, the desired RH can be achieved.

Acknowledgements

This research was supported by NSFC (no. 51322203, 51472111, 51202076), the National Program for Support of Top-notch Young Professionals, the Fundamental Research Funds for the Central Universities (no. lzujbky-2014-m02, lzujbky-2015-118, lzujbky-2015-208), and PCSIRT (no. IRT1251).

Notes and references

1 J. A. Paradiso and T. Starner, *IEEE Pervasive Comput.*, 2005, **4**, 18–27.
2 E. Bouendeu, A. Greiner, P. J. Smith and J. G. Korvink, *IEEE Sens. J.*, 2011, **11**, 107–113.
3 S. P. Beeby, M. J. Tudor and N. M. White, *Meas. Sci. Technol.*, 2006, **17**, 175–195.
4 M. S. Dresslhaus and I. L. Tomas, *Nature*, 2001, **414**, 332–337.
5 Z. L. Wang and J. H. Song, *Science*, 2006, **312**, 242–246.
6 Y. Qin, X. D. Wang and Z. L. Wang, *Nature*, 2008, **451**, 809–813.
7 Y. F. Hu, L. Lin, Y. Zhang and Z. L. Wang, *Adv. Mater.*, 2011, **10**, 5025–5031.
8 K. I. Park, J. H. Son, G. T. Hwang, C. K. Jeong, J. Ryu, M. Koo, I. Choi, S. H. Lee, M. Byun, Z. L. Wang and K. J. Lee, *Adv. Mater.*, 2014, **26**, 2514–2520.
9 S. B. Horowitz, M. Sheplak, L. N. Cattafesta III and T. Nishida, *J. Micromech. Microeng.*, 2006, **16**, 174–181.
10 X. D. Wang, J. H. Song, J. Liu and Z. L. Wang, *Science*, 2007, **316**, 102–105.
11 C. Xu, X. D. Wang and Z. L. Wang, *J. Am. Chem. Soc.*, 2009, **131**, 5866–5872.
12 S. N. Cha, J. S. Seo, S. M. Kim, H. J. Kim, Y. J. Park, S. W. Kim and J. M. Kim, *Adv. Mater.*, 2010, **22**, 4726–4730.
13 B. Li, J. H. You and Y. J. Kim, *Smart Mater. Struct.*, 2013, **22**, 055013.
14 R. Que, Q. Shao, Q. L. Li, M. Shao, S. D. Cai, S. D. Wang and S. T. Lee, *Angew. Chem., Int. Ed.*, 2012, **124**, 5514–5518.
15 N. Y. Cui, J. M. Liu, L. Gu, S. Bai, X. B. Chen and Y. Qin, *ACS Appl. Mater. Interfaces*, 2015, **7**, 18225–18230.
16 Y. B. Zheng, L. Cheng, M. M. Yuan, Z. Wang, L. Zhang, Y. Qin and T. Jing, *Nanoscale*, 2014, **6**, 7842.
17 F. R. Fan, L. Lin, G. Zhu, W. Z. Wu, R. Zhang and Z. L. Wang, *Nano Lett.*, 2012, **12**, 3109–3114.
18 G. Zhu, J. Chen, Y. Liu, P. Bai, Y. S. Zhou, Q. S. Jing, C. F. Pan and Z. L. Wang, *Nano Lett.*, 2013, **13**, 2282–2289.
19 L. Zhang, L. Cheng, S. Bai, C. Su, X. B. Chen and Y. Qin, *Nanoscale*, 2015, **7**, 1285–1289.
20 J. W. Zhong, Y. Zhang, Q. Z. Zhong, Q. Y. Hu, B. Hu, Z. L. Wang and J. Zhou, *ACS Nano*, 2014, **8**, 6273–6280.
21 Z. Wang, L. Cheng, Y. B. Zheng, Y. Qin and Z. L. Wang, *Nano Energy*, 2014, **10**, 37–43.
22 J. Yang, J. Chen, Y. Liu, W. Q. Yang, Y. J. Su and Z. L. Wang, *ACS Nano*, 2014, **8**, 2649–2657.
23 N. Y. Cui, L. Gu, J. M. Liu, S. Bai, J. W. Qiu, J. C. Fu, X. L. Kou, H. Liu, Y. Qin and Z. L. Wang, *Nano Energy*, 2015, **15**, 321–328.
24 J. M. Liu, N. Y. Cui, L. Gu, X. B. Chen, S. Bai, Y. B. Zheng, C. X. Hu and Y. Qin, unpublished work.
25 K. Y. Lee, J. Chun, J. H. Lee, K. N. Kim, N. R. Kang, J. Y. Kim, M. H. Kim, K. S. Shin, M. K. Gupta, J. M. Baik and S. W. Kim, *Adv. Mater.*, 2014, **26**, 5037–5042.
26 A. F. Yu, M. Song, Y. Zhang, L. B. Chen, J. Y. Zhai and Z. L. Wang, *Nano Res.*, 2015, **8**, 765–773.
27 K. N. Kim, J. Chun, J. W. Kim, K. Y. Lee, J. U. Park, S. W. Kim, Z. L. Wang and J. M. Baik, *ACS Nano*, 2015, **9**, 6394–6400.
28 V. Nguyen and R. S. Yang, *Nano Energy*, 2013, **2**, 604–608.
29 Y. Yang, H. L. Zhang, R. Y. Liu, X. N. Wen, T. C. Hou and Z. L. Wang, *Adv. Energy Mater.*, 2013, **3**, 1563–1568.